

LARGE HI STRUCTURES LINKED TO SOUTHERN O-TYPE STARS

M. C. Martín,¹ C. E. Cappa,^{1,2} and G. A. Romero^{1,2}

Received 2008 July 8; accepted 2008 October 1

RESUMEN

Analizamos la distribución del material interestelar en la vecindad de las estrellas de tipo O: HD 38666, HD 124979, HD 163758 y HD 171589, a fin de investigar la existencia de burbujas interestelares asociadas a las estrellas. La localización de las estrellas lejos del plano galáctico favorece la formación de burbujas de gran extensión. Con base en datos del HI, continuo de radio y CO, e imágenes en el infrarrojo lejano que revelan la emisión del polvo interestelar, investigamos la distribución del gas neutro e ionizado en estas regiones. Reportamos en este trabajo la detección de cavidades y envolturas en expansión en hidrógeno neutro, asociadas a las cuatro estrellas masivas. Se discute la posibilidad de que estas estructuras hayan sido originadas por la acción de los vientos estelares sobre el gas circundante.

ABSTRACT

In our search for interstellar bubbles around massive stars we analyze the environs of the O-type stars HD 38666, HD 124979, HD 163758, and HD 171589. The location of the stars, far from the galactic plane, favors the formation of large wind bubbles. We investigate the distribution of the neutral and ionized gas based on HI, CO, and radio continuum data, and that of the interstellar dust based on far infrared IRIS images. Here we report the discovery of neutral gas cavities and slowly expanding shells associated with the four massive stars. IR and optical counterparts were also detected for some of the stars. We discuss the probability that the features have originated by the action of stellar winds on the surrounding gas.

Key Words: ISM: bubbles — stars: individual (HD 38666, HD 124979, HD 163758, HD 171589)

1. INTRODUCTION

The strong stellar winds of massive stars interact with their environs creating *interstellar bubbles* that are detected over a large range of wavelengths. UV photons with energies $h\nu \geq 13.6$ eV ionize the inner part of the expanding bubbles, which are generally detected both in the optical (Lozinskaya 1982) and in the radio continuum ranges as shell-like thermal sources (Goss & Lozinskaya 1995). Should the ionizing front be trapped within the expanding envelope, interstellar bubbles will have an outer neutral region that can be identified both in the HI 21-cm line emission and in molecular lines (Cappa et al. 2005).

Many interstellar bubbles are detected neither in the radio continuum nor in optical lines (e.g. Cappa

& Benaglia 1998; Arnal et al. 1999; Cichowski & Arnal 2004). A low ambient density may be responsible for the undetected radio continuum or optical emission, as was suggested for bubbles in the LMC by Nazé et al. (2002). As a consequence, the analysis of the HI emission distribution is an important tool to investigate the presence of such structures and allows discrimination in distance based on galactic rotation models.

Data at radio and infrared wavelengths offer an opportunity to investigate the characteristics and distribution of the ionized and neutral gas associated with these bubbles, as well as those of the interstellar dust.

A low-velocity massive star with constant stellar wind parameters located in a homogeneous interstellar medium with uniform density creates a spherical stellar wind bubble. Aspherical bubbles appear

¹Instituto Argentino de Radioastronomía (IAR-CONICET), Argentina.

²Facultad de Ciencias Astronómicas y Geofísicas, Universidad Nacional de La Plata, Argentina.

as the result of relaxing some of these hypotheses. The combination of a powerful stellar wind and a high space velocity changes this scenario drastically. Weaver et al. (1977) pointed out that a massive star moving supersonically with respect to the surrounding gas originates an aspherical stellar bubble, elongated in the direction of the movement of the star. A wind bow-shock can develop ahead of the star (Wilkin 1996; Raga et al. 1997). As van Buren & McCray (1988) have shown, these shocks can be identified by their far IR emission.

Here we present a large scale study of the interstellar medium around four southern O-type stars: HD 38666, HD 124979, HD 163758, and HD 171589, the first two of them classified as runaway stars. Our aim is to investigate the action of the UV photon flux and the stellar winds of these stars on their surroundings. The selected stars are located at $|b| > 3^\circ$, allowing for the formation of relatively large structures which are easily identified using low angular resolution data.

In the following sections, we analyze the interstellar medium in the environs of the stars, looking for cavities and shells in the neutral gas that have originated by the action of the massive stars on their surroundings. These studies are important to improve theoretical models on the interplay between massive stars and the surrounding gas.

2. DATA BASES

The HI 21-cm line data analyzed in this paper were extracted from the Leiden Argentine Bonn Survey of Galactic HI (Kalberla et al. 2005; Arnal et al. 2000) observed using the radiotelescope of the Instituto Argentino de Radioastronomía. The 21-cm data span the velocity range from -250 to $+250$ km s $^{-1}$ and were obtained with a velocity resolution of 1.3 km s $^{-1}$. The angular resolution is $30'$.

Radio continuum data at 4.85 GHz from the Parkes-MIT-NRAO (PMN) Southern Radio Survey (Condon, Griffith, & Wright 1993) are available only for HD 124979 and HD 171589, while data at 408 MHz (Haslam et al. 1982) and at 35 MHz (Dwarakanath & Udaya-Shankar 1990) are available for the four target stars. The angular resolutions are $5'$, $0.85'$, and $26' \times 42' / \cos(\delta - 14^\circ)$, for the surveys at 4.85 GHz, 408 MHz, and 35 MHz, respectively.

The analysis of the molecular gas distribution for the regions of HD 163758 and HD 171589 was based on the CO survey by Dame, Hartmann, & Thaddeus (2001), which has an angular resolution of $8.8'$. The velocity coverage and the velocity resolution are -160 to $+160$ km s $^{-1}$ and 1.3 km s $^{-1}$, respectively. The rms noise level is 0.2 K.

The dust distribution in the region was analyzed using the IRIS³ database. These images are a new generation of IRAS images that benefit from a better zodiacal light subtraction, calibration, and a better destripping. IRIS images have an angular resolution of around $4'$ (Miville-Deschênes & Lagache 2005).

The optical images were obtained from the Full-Sky H-Alpha survey (H-Alpha Composite, Finkbeiner 2003).

3. TARGET STARS

Table 1 summarizes the stellar parameters relevant to this study: the name of the stars and their galactic coordinates are listed in the first two columns. The spectral types, indicated in the third column, were obtained from Maíz-Appellániz et al. (2004) (GOS catalogue). Distance estimates taken from the literature are given in Column 4. Columns 5 and 6 list the visual magnitudes V and color indices $(B - V)$, respectively. We used these values together with absolute magnitudes from Vacca, Garmany, & Shull (1996) and intrinsic color indices from Wegner (1994) to derive the spectrophotometric distance listed in Column 7. The components of the proper motion in the galactic coordinate system listed in Columns 8 and 9 were calculated from the Tycho-2 catalogue (Høg et al. 2000). Finally, z -distances to the galactic plane are shown in Column 10. They were derived by adopting the distances listed in Column 7.

Based on its large proper motion, HD 38666 (μ Col) was identified as a runaway star belonging to Ori OB1 (Blaauw 1961).

HD 124979 has been classified as an O8 ((f)) star by MacConnell & Bidelman (1976). Following the Of typification by Walborn (1971), we have adopted a luminosity class III. Mason et al. (1998) analyzed the binarity status, and concluded that it maybe a spectroscopic binary, tagging it as “SB1?”. The measured proper motion and radial velocity (-68 km s $^{-1}$) allow us to classify this star as a runaway.

No information about the interstellar medium in the environs of the target stars was found in the literature.

4. HI EMISSION TOWARDS THE SELECTED STARS

Figure 1 (a-d) displays the HI 21-cm line profiles towards the O-type stars. They were obtained by averaging the HI emission within an area of about $3^\circ \times 3^\circ$ centered at the position of the massive stars.

³<http://www.ias.fr/IRIS>.

TABLE 1
MAIN PARAMETERS OF THE O-TYPE STARS

(1)	(2)	(3)	(4)	(5)	(6)	(7)	(8)	(9)	(10)
Name	(l, b)	Spectral Classification	d	V	$(B - V)$	d_{spc}^e	$\mu_l \cos b^f$	μ_b^f	z
	($^\circ$)		(kpc)	(mag)	(mag)	(kpc)	(mas yr $^{-1}$)	(mas yr $^{-1}$)	(pc)
HD 38666	237.29, -27.10	O9.5 V ^a	0.53 ^a	5.17 ^a	-0.27 ^a	0.8	+23.48±1.1	-3.52±1.1	-255
HD 124979	316.40, +9.08	O8 III ((f)) ^b		8.52 ^a	1.05 ^a	3.7	-8.8±1.1	+8.2±1.1	+590
HD 163758	355.36, -6.10	O6.5 Ia (f) ^a		7.32 ^a	0.03 ^a	3.5	-2.5±1.5	-5.2±1.5	-374
HD 171589	18.65, -3.09	O7 II (f) ^a	1.15 ^c -1.5 ^d	8.29 ^a	0.29 ^a	3.0	+6.0±1.5	-4.1±1.5	+160

^aGOS catalogue (Maíz-Apellániz et al. 2004).

^bSee text.

^cKozok (1985).

^dGarmany, Conti, & Chiosi (1982).

^eSpectrophotometric distances derived in this paper. See text for details.

^fDerived from Tycho-2 catalogue (Høg et al. 2000).

Our aim is to analyze the main characteristics of the neutral gas emission towards the selected stars and its relation to the galactic spiral structure.

The HI emission profile in the region of HD 38666 (Figure 1a) reveals a weak HI gas component centered at $v \approx 0$ km s $^{-1}$ (all velocities in this paper are referred to the LSR). Because of the high galactic latitude of the star, this material corresponds to local gas. Bearing in mind the distances to HD 38666 listed in Table 1, we expect gas related to this star to have low positive velocities.

The HI emission profile in the region of HD 124979 (Figure 1b) reveals three components centered at $v \approx -2$, $v \approx -20$, and $v \approx -50$ km s $^{-1}$. The former gas component is associated with the local region. The circular galactic rotation model by Brand & Blitz (1993) predicts near and far kinematical distances $d \approx 1.4$ and 11 kpc, respectively, for the component at -20 km s $^{-1}$, while for the component at -50 km s $^{-1}$, $d \approx 3.7$ and 8.5 kpc, respectively. The near kinematical distances are compatible with the locations of the Sagittarius-Carina and Scutum-Crux spiral arms (Russeil 2003). According to the analytical fit by Brand & Blitz (1993), gas in the environs of this star, i.e. at 3.7 kpc, should have velocities of about -50 km s $^{-1}$.

In the line of sight to HD 163758 (Figure 1c), HI emission was detected from -40 to $+40$ km s $^{-1}$. The profile shows a main peak of neutral gas emission centered at $v \approx +5$ km s $^{-1}$, probably related to the local spiral arm. The fact that positive velocities are forbidden in the fourth galactic quadrant within the solar circle (e.g. Brand & Blitz 1993) indicates

that most of this material is local and is associated with Gould's belt (Olano 1982). Gas linked to this star at a distance of 3.5 kpc should have velocities of about -10 km s $^{-1}$. Note however that kinematical distances have large uncertainties in this line of sight.

The HI emission towards HD 171589 (Figure 1d) was detected within the velocity interval -40 to $+100$ km s $^{-1}$. The neutral gas emission shows major peaks at $v \approx 0$, $v \approx +12$ km s $^{-1}$, and $v \approx +40$ km s $^{-1}$. The lower velocity peak belongs to the local spiral arm, while peaks at positive velocities correspond to near and far kinematical distances $d \approx 1.3$ and 15 kpc, and $d \approx 3.4$ and 12.5 kpc, respectively. These gas components are probably related to the Sagittarius-Carina and Scutum-Crux spiral arms, respectively (Russeil 2003). A relatively low emission component can also be identified at ≈ -25 km s $^{-1}$. The analytical fit by Brand & Blitz (1993) predicts that gas with this velocity is located at ≈ 20 kpc, well beyond the solar circle. Material related to the star, placed at $d \leq 3$ kpc, should appear with velocities lower than $+33$ km s $^{-1}$.

5. HI STRUCTURES AND THEIR COUNTERPARTS AT OTHER FREQUENCIES

In order to look for HI structures linked to the selected stars, we analyzed the neutral hydrogen distribution in their environs. A series of (l, b) maps at maximum velocity resolution (1.3 km s $^{-1}$) showing the HI emission distribution at different velocities were constructed. Although the whole velocity range at which HI emission is detected was analyzed, the

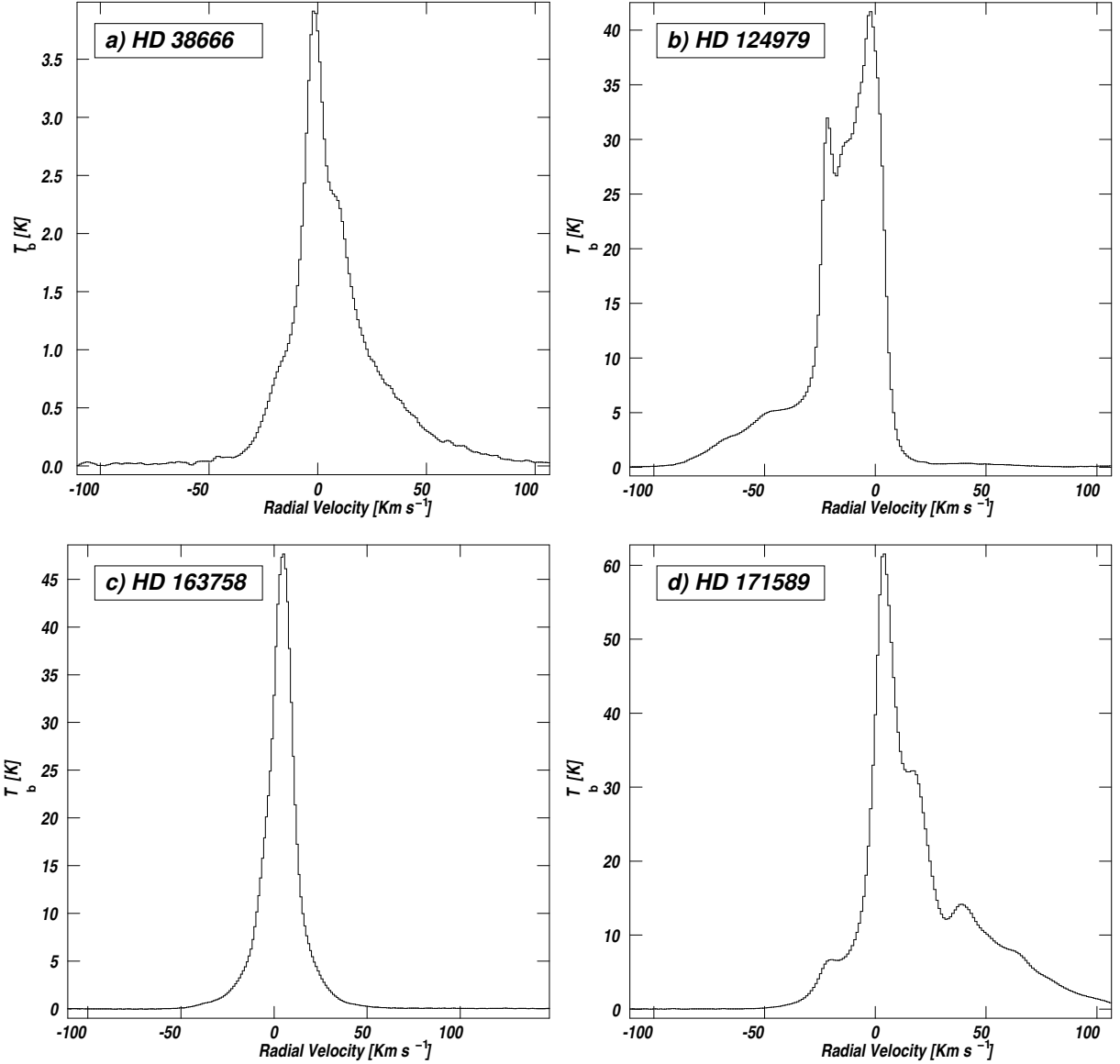


Fig. 1. HI profiles obtained by averaging the HI emission in regions of $3^\circ \times 3^\circ$ around the O-type stars. (a) HD 38666; (b) HD 124979; (c) HD 163758; and (d) HD 171589. The intensity scale is given as a brightness temperature. Velocities are referred to the LSR.

figures include only the images where HI structures probably linked to the stars are detected.

The identification of an HI structure associated with a certain star requires a careful inspection of the HI images, looking for shells and voids that might be related to the star. Several conditions are necessary to associate an HI structure with a certain star: (a) the star is expected to be located inside the HI void or close to its inner borders; (b) the kinematical distance to the structure should coincide, within errors, with the spectrophotometric distance; and (c) bearing in mind that the velocity dispersion in the

interstellar medium is about 6 km s^{-1} , an HI feature should remain detectable for a larger velocity interval to be considered as a physical structure.

We have found a number of HI structures towards the target stars that fulfill these conditions and, consequently, can be related to the stars. In the following sections we describe the HI structures along with their counterparts at other wavelengths.

The main physical parameters of each structure are summarized in Table 2, which is described in § 6.1.

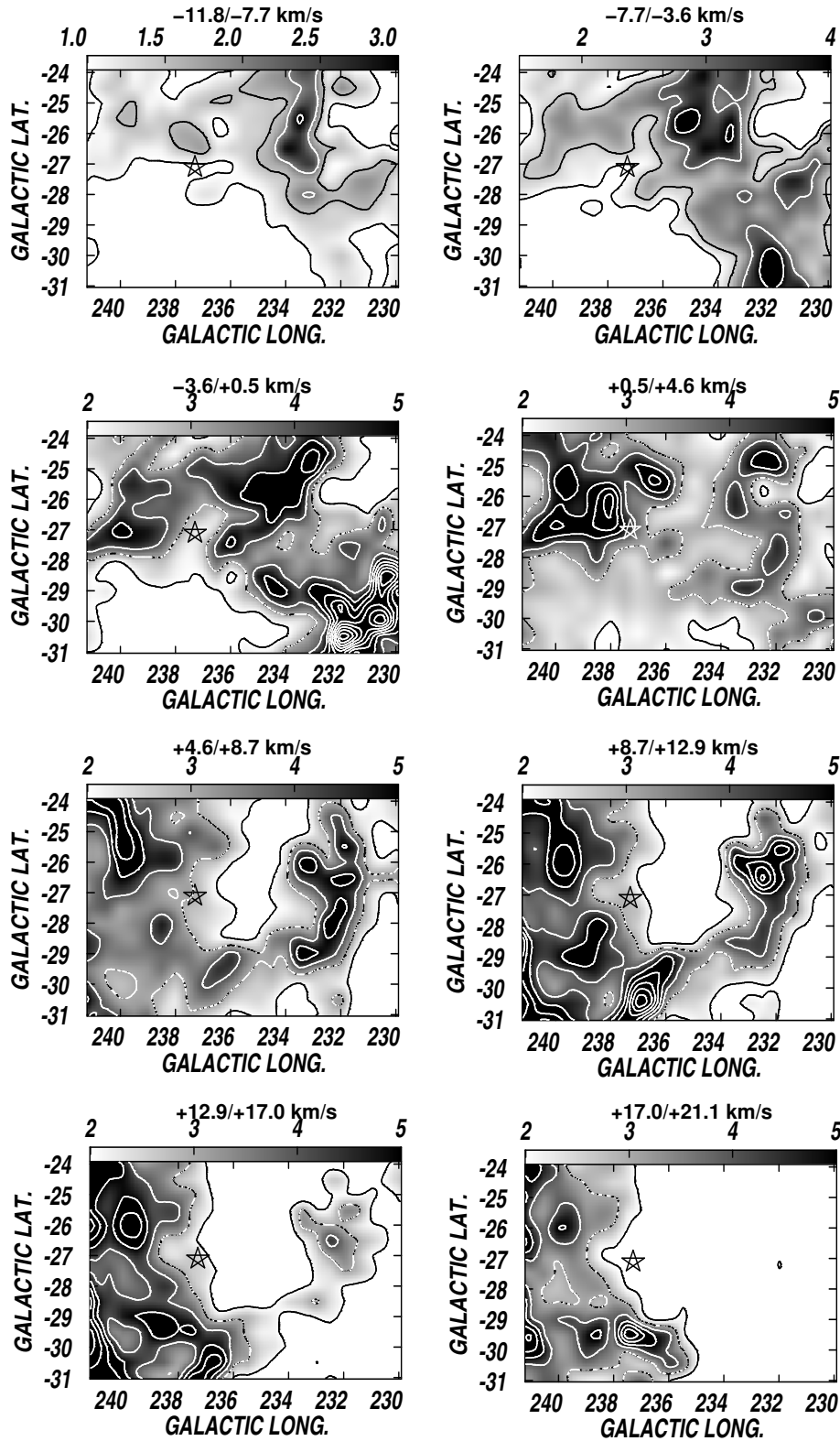


Fig. 2. HI emission distribution towards HD 38666, integrated in steps of 4 km s^{-1} . The velocity range and the greyscale (in K) of each image are indicated in its upper part. The contour lines go from the minimum value of the grayscale to 12 K, in steps of 1 K. HD 38666 is indicated by the star.

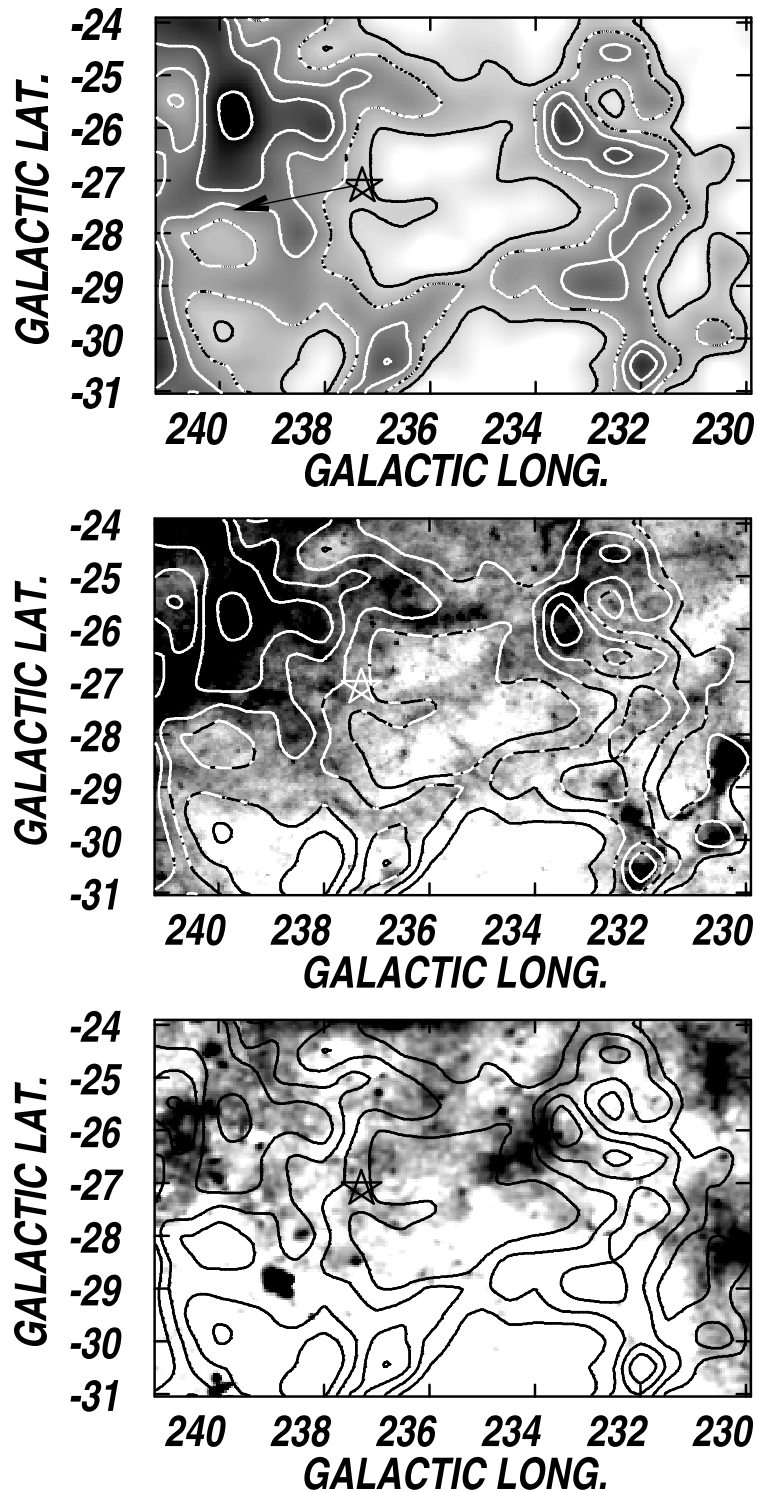


Fig. 3. Upper panel. HI emission distribution within the velocity interval -7.2 to $+17.0$ km s^{-1} showing the HI structure related to HD 38666. The grayscale goes from 2 to 5 K, and the contour lines are 2.5, 3, 3.5, 4 and 5 K. HD 38666 is indicated by a star. Central panel. Overlay of the IR emission at $100 \mu\text{m}$ (grayscale) and the same HI contours of the upper panel. The grayscale corresponds to 1.8 to 2.8 MJy ster^{-1} . Bottom panel. Overlay of the H α composite image (grayscale) and the same HI contours of the upper panel. The grayscale goes from 4.3 to 6.5 R.

5.1. The ISM around HD 38666

The HI emission distribution towards this star within the velocity interval from -11.8 to $+21.1$ km s $^{-1}$ is displayed in Figure 2. HD 38666 is indicated by a star. The images show that the O-type star is projected onto the border of a low emission region identified within the velocity interval from -7.7 to $+17.0$ km s $^{-1}$, centered approximately at $(l, b) = (235^\circ.5, -27^\circ.5)$. Identification of HI structures is difficult for velocities higher than $+17$ km s $^{-1}$ due to the lower general HI emission in the region.

The cavity and surrounding shell around this star is shown in Figure 3 (upper panel). The image was obtained by integrating the HI emission within the velocity interval from -7.7 to $+14.0$ km s $^{-1}$. The feature is elongated in the direction of the stellar proper motion, which is marked in the figure with a black arrow. The central panel displays an overlay of the IRIS image at $100 \mu\text{m}$ (grayscale) and the HI image (contour lines). The HI shell can partially be detected in the far infrared. The presence of a strong IR filament at $b \approx -25^\circ$ is compatible with the existence of a thin HI wall in this region. An IR emission band is also projected onto the cavity. If related to the structure, this emission might be linked to the approaching or receding caps.

The bottom panel shows a superposition of the same HI contour lines and the H α composite image. Optical emission is present inside the cavity and appears bordered by the neutral envelope towards lower galactic longitudes and higher negative galactic latitudes.

Neither catalogued HII regions nor supernova remnants were found over the regions under study. The image at 408 MHz (not shown here) displays a ring-like structure centered at $(l, b) = (235^\circ.0, -28^\circ.0)$, with inner and outer semiaxes of $2^\circ.1 \times 0^\circ.7$ and $4^\circ.2 \times 1^\circ.9$, respectively. The radio continuum feature is clearly larger than the HI cavity, and most of it is projected onto the neutral envelope, contrary to what is expected for an interstellar bubble or an HII region. Thus, the lack of coincidence between the radio continuum feature and the HI cavity casts doubts on its relation to the neutral shell.

The systemic velocity of the structure, defined as the velocity at which the cavity has its larger dimensions and is better defined, is $+8$ km s $^{-1}$. According to the analytical fit by Brand & Blitz (1993), the low systemic velocity derived for the HI structure indicates a kinematical distance of about 1.0 kpc, in agreement with the stellar distance listed in Table 1. The location of the star with cavity, together with the agreement between the kinematical

and spectrophotometric distances strongly suggest that the HI structure is related to HD 38666. We have adopted a distance $d = 0.5 \pm 0.1$ kpc for this structure.

At this distance, the stellar tangential velocity is quite large, $v_t \approx 57 \pm 15$ km s $^{-1}$, and the massive star could have created a bow-shock structure. The presence of a bow-shock like object related to this star was investigated by van Buren & McCray (1988), who were not successful in finding such a structure in the IRAS images.

5.2. The ISM around HD 124979

The analysis of the HI emission distribution maps towards HD 124979 allows identification of a cavity and shell probably associated with the star (Figure 4). The HI minimum is detected within the velocity interval from -52.0 to -23.2 km s $^{-1}$, decreasing in angular size for velocities $v > -31.4$ km s $^{-1}$. At the stellar position, the contour lines are distorted in the velocity range -52.0 to -39.7 km s $^{-1}$.

The HI minimum is better defined from -52.0 to -31.4 km s $^{-1}$, and thus the systemic velocity of the structure can be derived as the central value of the mentioned interval, $v_{\text{sys}} \approx -42 \pm 10$ km s $^{-1}$. Taking into account a velocity dispersion of 6 km s $^{-1}$, the systemic velocity corresponds to a kinematical distance of 3.0 ± 1.0 kpc, which is compatible with the spectrophotometric distance. We have adopted $d = 3.5 \pm 1.0$ kpc as the distance to the HI structure.

Figure 5 (upper panel) shows the HI brightness temperature distribution towards HD 124979, averaged over the velocity interval from -47.9 to -35.6 km s $^{-1}$, for which the HI cavity is better defined. In order to delineate the cavity we have considered the brightness temperature contour corresponding to 3.5 K. The centroid of the structure is $(l, b) = (317^\circ.2, +9^\circ.3)$. Both the cavity and the almost complete shell are elongated in the direction of the tangential motion of the star (marked with a black arrow).

The $100 \mu\text{m}$ IRIS image shows far IR emission bordering the region towards the galactic plane, revealing the presence of dust associated with the bright portions of the surrounding shell (Figure 5, central panel). The bright IR areas detected inside the cavity, which extend well beyond the cavity, are probably unrelated to the HI structure. The proper motion of the star corresponds to a tangential velocity of $v_t \approx 200 \pm 30$ km s $^{-1}$. A careful inspection of the IRIS images does not allow the detection of a bow-shock-like structure at IR wavelengths.

Neither catalogued HII regions nor supernova remnants are linked to the structure. The bottom

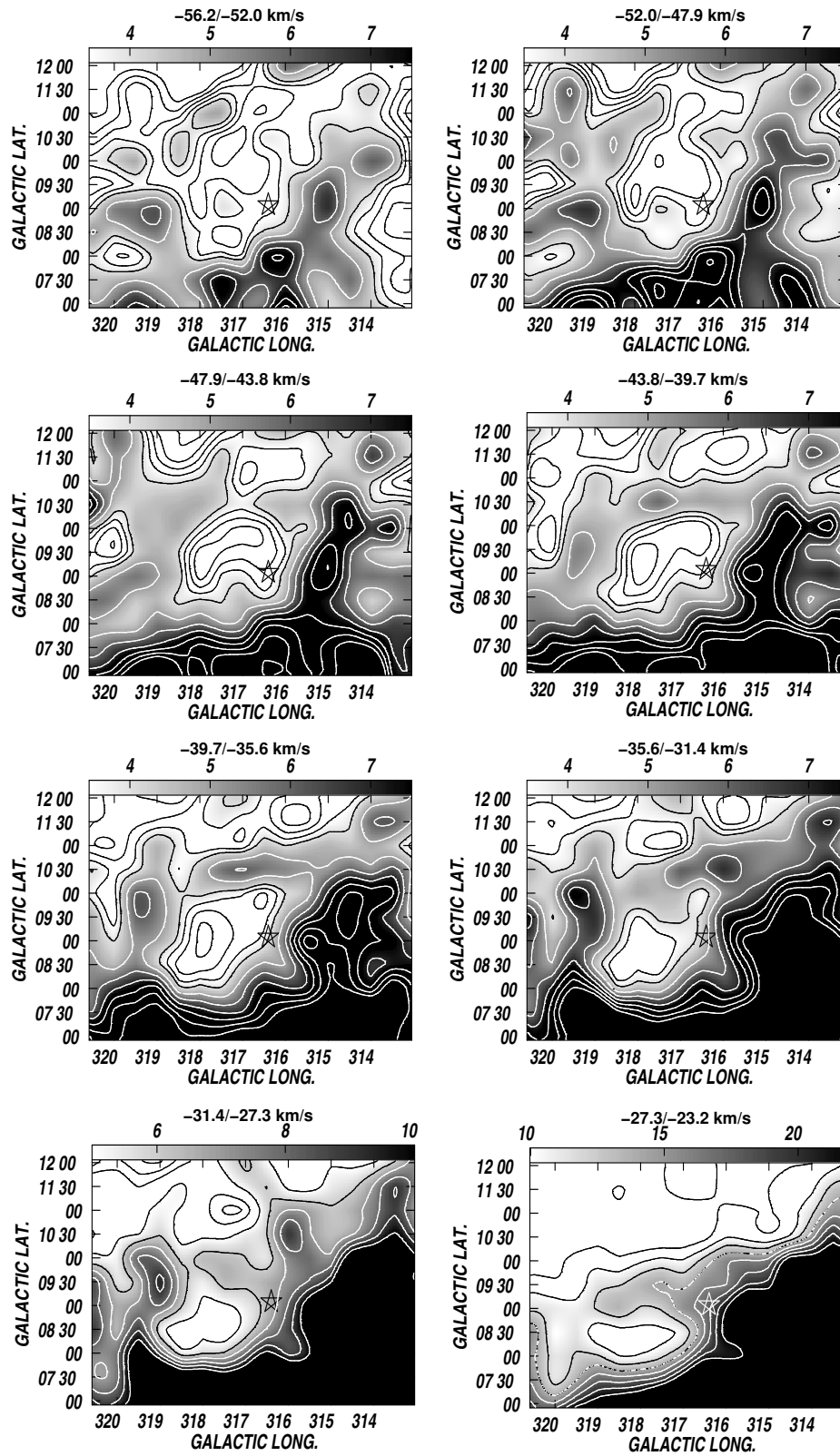


Fig. 4. HI emission distribution towards HD 124979, as in Figure 2. For the seven first maps, the contour lines go from 2 to 4 in steps of 0.5 K and for 5 to 10 in steps of 1 K, and for the last map, from 8 to 22 in steps of 2 K.

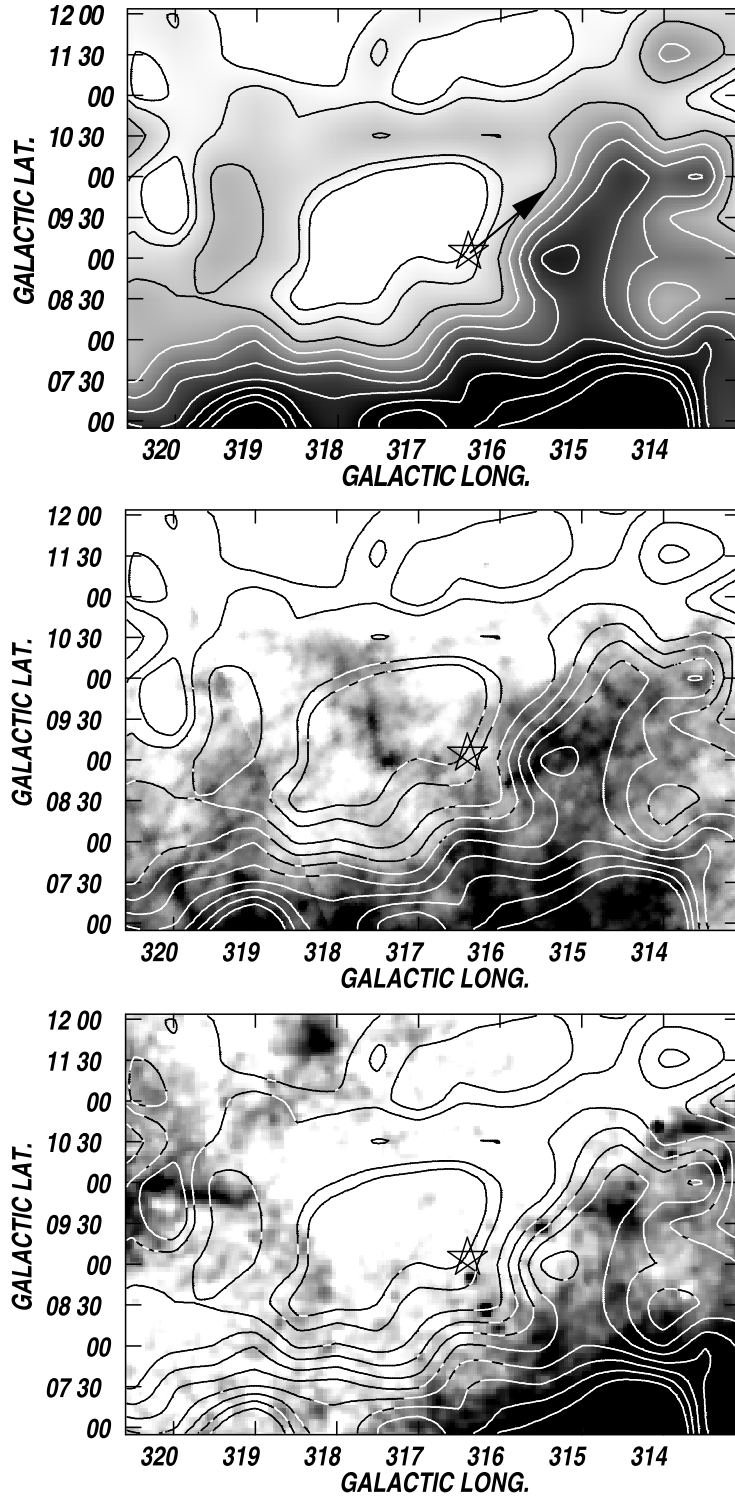


Fig. 5. Upper panel. Probable H I structure related to HD 124979. The image shows the H I column density distribution within the velocity interval $-47.9, -34.6 \text{ km s}^{-1}$. The grayscale goes from 3.5 to 10 K, and the contour lines go from 3.5 K to 12 K in steps of 1 K. Central panel. Overlay of the far IR emission distribution at $100 \mu\text{m}$ (grayscale from 21 to 35 MJy ster^{-1}) and the H I column density distribution (*contour lines*). Bottom panel. Overlay of the H α composite image (grayscale) from 10 to 14 R and the H I column density distribution (*contour lines*).

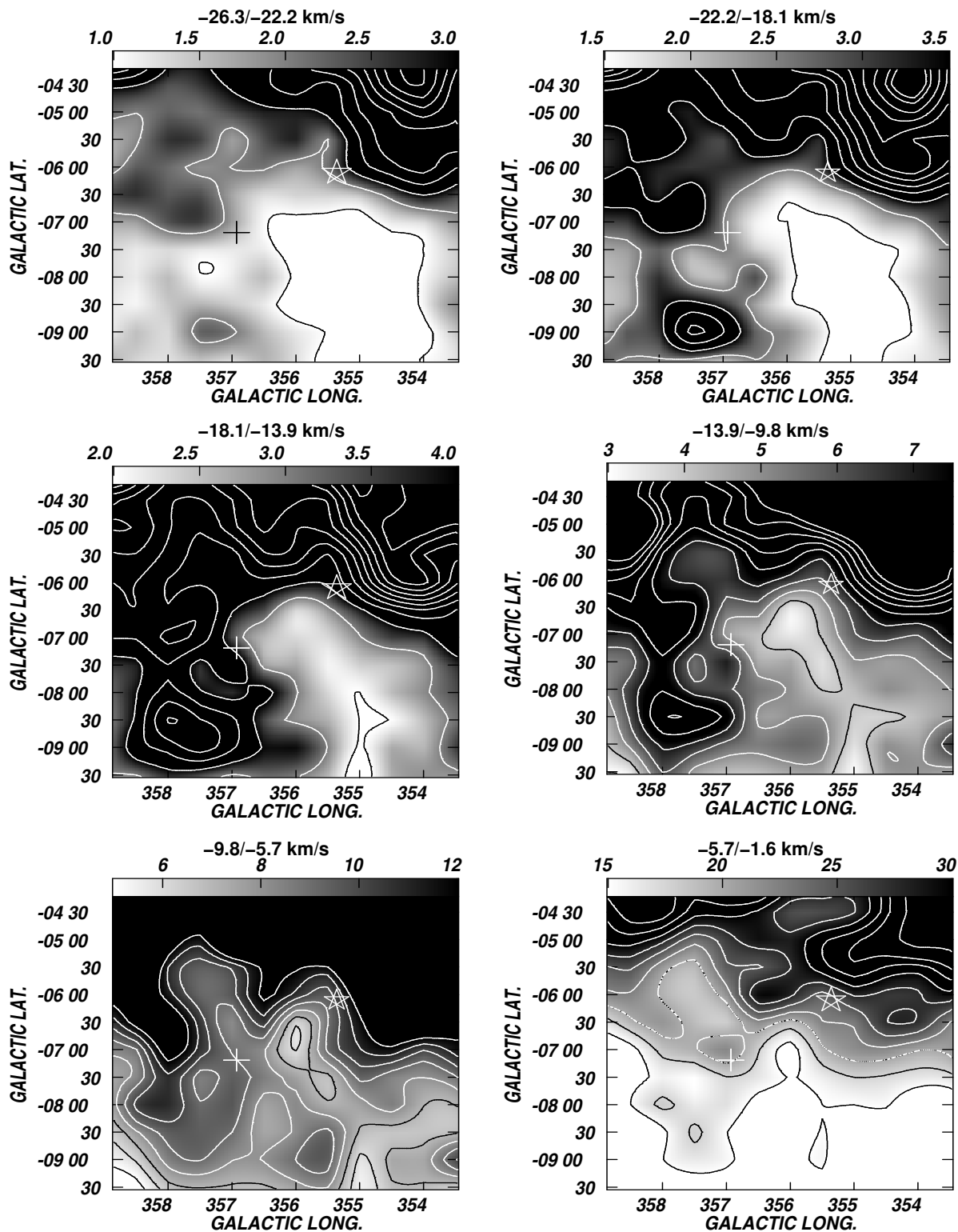


Fig. 6. H I emission distribution towards HD 163758, as in Figure 2. For the maps corresponding to the interval -26.3 to -5.7 km s $^{-1}$, the contour lines go from the minimum value of the grayscale to 12 K, in steps of 1 K. For the image showing the interval -5.7 to -1.6 km s $^{-1}$, the contour lines go from the minimum value of the grayscale to 40 K, in steps of 2.5 K. HD 163658 and WR 109 are indicated by the star and the cross, respectively.

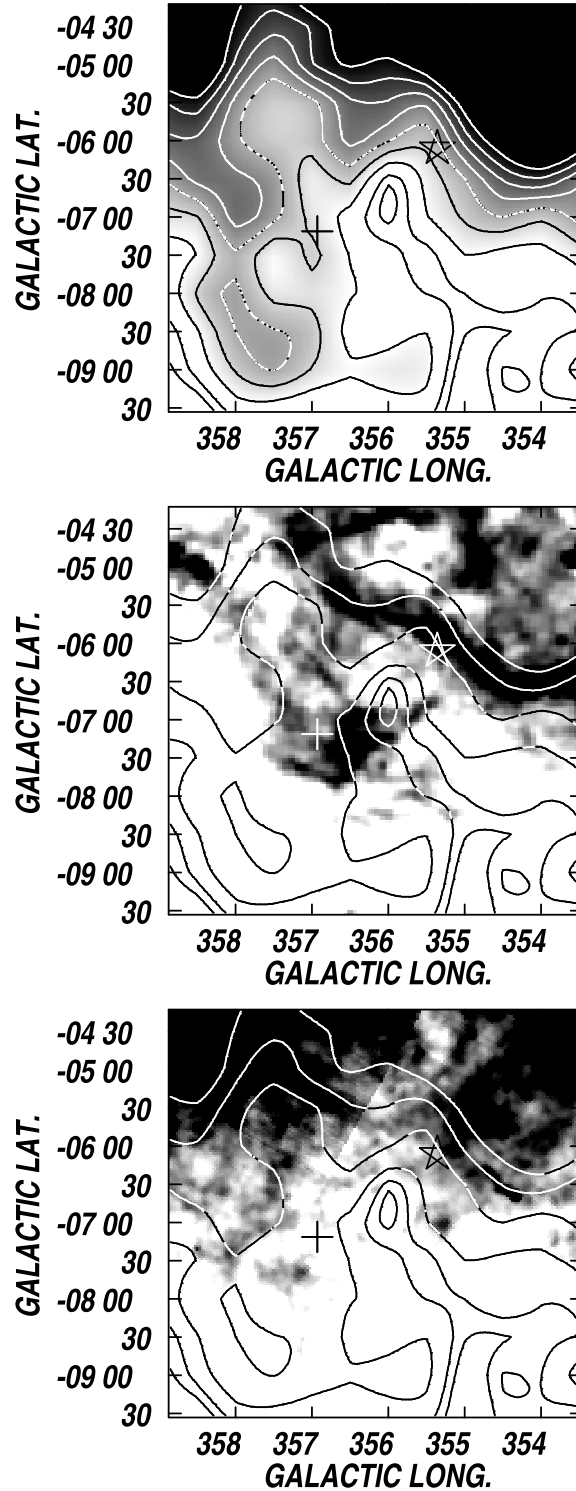


Fig. 7. Upper panel: HI emission towards HD 163758 integrated within the velocity range -22.2 to -5.7 km s $^{-1}$. The grayscale goes from 6 to 12 K. The contour lines go from 4.5 and 5 to 12 K, in steps of 1 K. Central panel: Overlay of the H α composite image (grayscale from 32 to 45 R) and the HI emission (contour lines, 4.5, 5 and from 6 to 12 K, in steps of 2 K). Bottom panel: Overlay of the IR emission at 100 μ m (grayscale from 50 to 80 MJy ster $^{-1}$) and the HI emission contour lines of central panel.

panel of Figure 5 indicates that no significant optical emission is detected towards this region. An inspection of the image at 408 MHz does not show identifiable radio emission probably related to the HI structure.

No additional OB stars at a compatible distance are projected onto the HI structure.

5.3. *The ISM around HD 163758*

Figure 6 displays HI brightness temperature images corresponding to the velocity interval from -26.3 to -1.6 km s $^{-1}$ in the vicinity of HD 163758. An inspection of the images shows the presence of a low emission region at $b \leq -5^\circ$.

The HI cavity centered at $(l, b) = (356^\circ 0, -6^\circ 5)$ can be appreciated at velocities in the range v from -26.3 to -5.7 km s $^{-1}$. HD 163758, which is indicated by the star symbol, appears projected near the higher density border of the cavity, indicated by the pile-up of the contour lines.

The upper panel of Figure 7 displays the mean HI brightness temperature in the range $(-22.2, -5.7)$ km s $^{-1}$, where the cavity and shell centered at $(l, b) = (356^\circ 0, -6^\circ 5)$ are clearly identified in contours and grayscale. The central and bottom panels show overlays of the HI emission distribution and the H α and 100 μ m IRIS emissions, respectively. The H α image reveals a shell-like structure of about $1^\circ 5$ in diameter centered at $(l, b) = (356^\circ 0, -6^\circ 5)$, with the O-type star projected onto one of its borders. The IRIS image shows the lack of IR emission in the region of the HI cavity. Bearing in mind the angular resolution of the HI data, the correlation of the optical feature with the small HI structure is good, suggesting that the HI feature is the neutral gas counterpart of the optical shell. The fact that the star appears projected onto the highest density border of the HI structure reinforces the association between the star and the cavity.

A search for other massive stars projected onto the region shows that the Wolf-Rayet star WR 109 (= V617 Sgr, WN5h+?, van der Hucht 2001) is placed about 2° far away from the position of the O star. According to van der Hucht (2001), WR 109 is located at a photometric distance of 34 kpc. The large estimated distance is the result of the low optical absorption derived for the star, along with its low apparent magnitude. This WR star, marked by a cross in Figures 6 and 7, is also near the border of the cavity. Its position, well outside the optical shell, suggests that the WR star is unconnected to the H α shell.

The systemic velocity of the HI structure is -10 ± 1 km s $^{-1}$. The analytical fit to the circular

galactic rotation model predicts that material at velocities of about -10 km s $^{-1}$ is placed at near and far kinematical distances of 3.3 ± 1.0 and 13–14 kpc, respectively. The near kinematical distance agrees with the spectrophotometric distance to HD 163758 (see Table 1). Note that kinematical distances have large uncertainties in this section of the Galaxy. We adopt 3.5 ± 1.0 kpc as the distance to the HI feature.

According to SIMBAD, no HII regions or SNR have been identified in this area. No additional OB stars were found projected onto the HI structure. The analysis of the CO images by Dame et al. (2001) did not show detectable molecular emission in this region.

5.4. *The ISM around HD 171589*

Figure 8 displays the HI emission distribution within the velocity interval from $+20.1$ to $+57.2$ km s $^{-1}$ in a large area around the massive star. Two cavities are clearly detected for velocities in the range $+26$ to $+45$ km s $^{-1}$, centered at $(l, b) = (18^\circ 7, -3^\circ 0)$ and $(17^\circ 5, -2^\circ 7)$. HD 171589 appears projected onto the cavity at larger galactic longitudes.

The upper panel of Figure 9 displays the HI column density distribution within the velocity range from $+26.3$ to $+44.8$ km s $^{-1}$. Both cavities are separated in this image. The O-type star is projected onto the HI hole at $(l, b) = (18^\circ 7, -3^\circ 0)$, partially surrounded by an HI shell.

The central and bottom panels of Figure 9 show the superposition of the HI column density image (in contours) and the H α and IRIS images, respectively. The central panel reveals a region without optical emission coincident with the cavity at $(l, b) = (18^\circ 7, -3^\circ 0)$. The bottom panel shows that both HI holes are partially outlined by bright IR emission at $b > -3^\circ 5$. The distribution of the HI, optical, and IR emissions is compatible with the presence of an interstellar bubble driven by the massive star.

The systemic velocity of the structure at $(l, b) = (18^\circ 7, -3^\circ 0)$ is $+36 \pm 2$ km s $^{-1}$, corresponding to near and far kinematical distances of 3.2 ± 0.5 and 13 kpc, respectively. The near kinematical distance agrees with the spectrophotometric distance derived for the star. Consequently, we adopt $d = 3.0 \pm 0.5$ kpc.

Six supernova remnants were detected in this area at galactic latitudes $b \geq -2.8$ (Green 2002). Two of them (G17.4-2.3 and G17.8-2.6) appear projected onto the cavity centered at $(l, b) = (17^\circ 5, -2^\circ 7)$. Based on the Σ -D relation, Guseinov, Ankaev, & Tagieva (2003) derived distances of about 6.3 kpc to the SNRs. As discussed by many authors

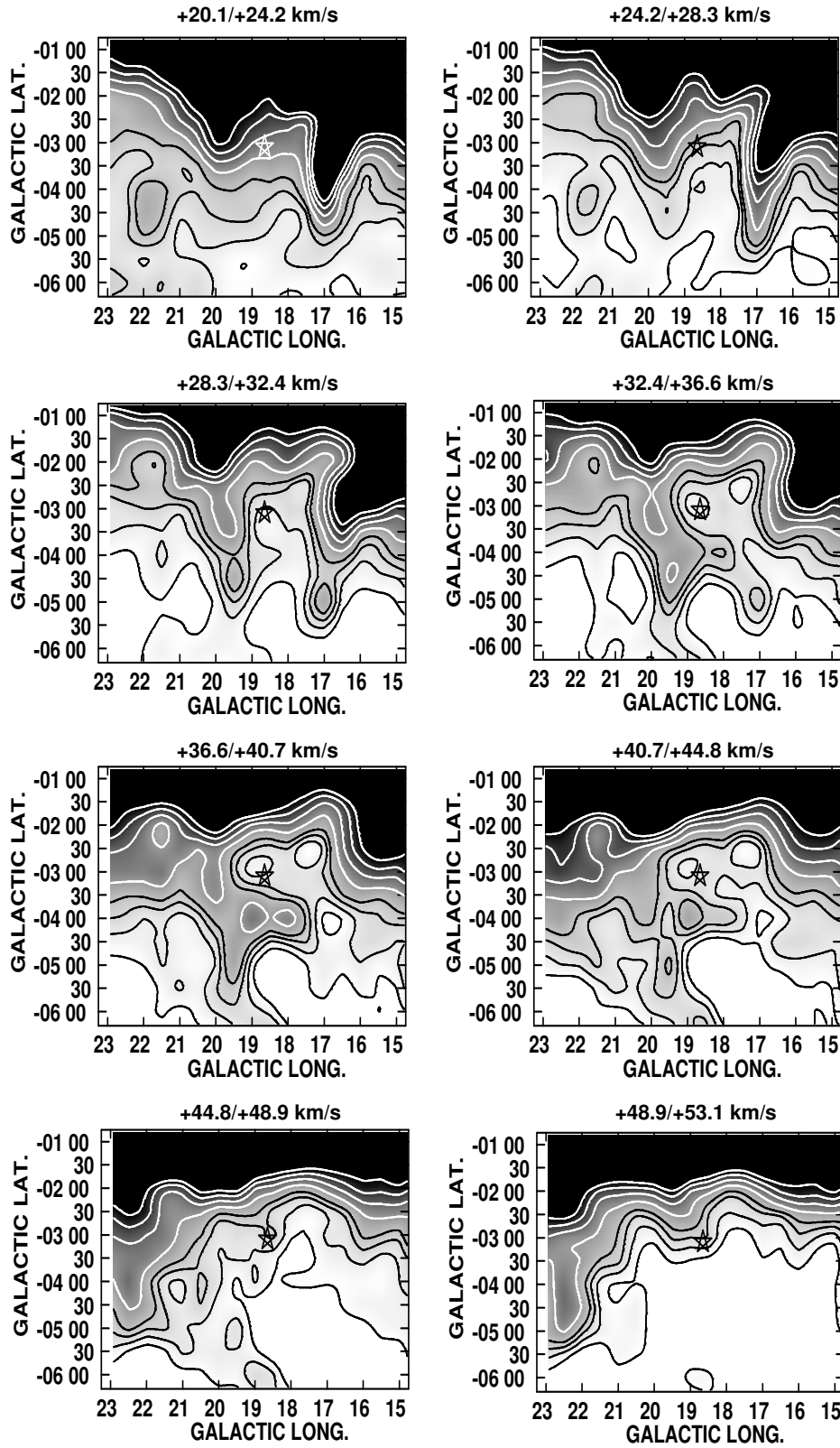


Fig. 8. H I emission distribution towards HD 171589, as in Figure 2. The grayscale goes from 5 to 30 K. The contour lines go from 5 to 11 K, in steps of 2 K, and from 15 to 30 K, in steps of 5 K.

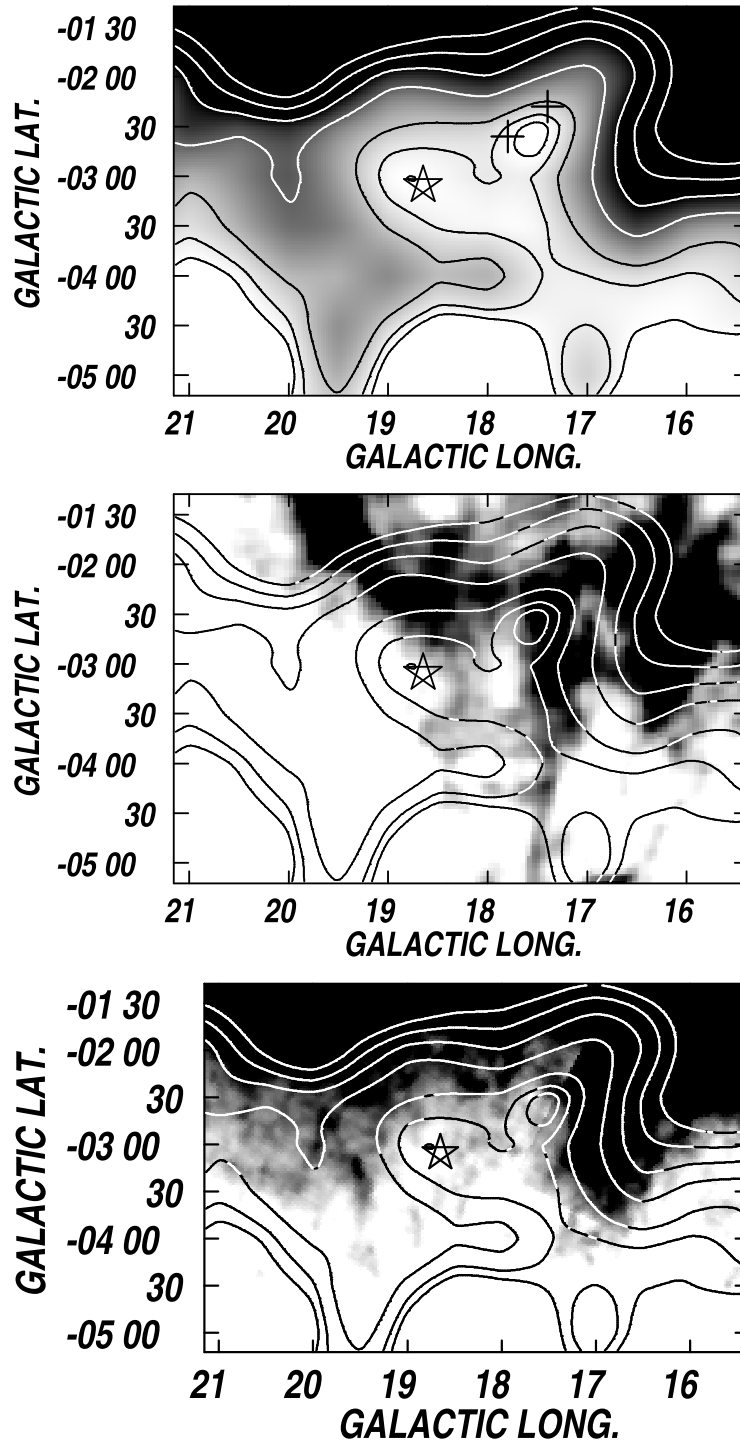


Fig. 9. Upper panel: HI column density distribution towards HD 171589, within the velocity range $+26.3$ to $+44.8$ km s^{-1} . The grayscale goes from 7 to 20 K. Contour lines go from 7, 8, and 10 K, and from 15 to 30 K, in steps of 5 K. HD 171589 is indicated by a five pointed star, and the SNR G17.4-2.3 and SNR G17.8-2.6 are marked by crosses. Central panel: Overlay of the H α composite image (grayscale from 35 to 70 R) and the HI column density distribution shown in the upper panel (contour lines). Bottom panel: Overlay of the IR emission distribution at $100 \mu\text{m}$ (grayscale from 70 to 130 MJy ster^{-1}) and the HI column density distribution shown in the upper panel (contour lines).

TABLE 2
PHYSICAL PARAMETERS OF THE HI STRUCTURES AROUND THE O STARS

	HD 38666	HD 124979	HD 163758	HD 171589
(l, b) center	(235°5, -27°5)	(317°2, +9°3)	(356°0, -6°5)	(18°7, -3°0)
Velocity interval v_1, v_2 (km s ⁻¹)	-7, +17	-53, -25	-22, -5	+26, +45
Systemic velocity v_{sys} (km s ⁻¹)	+8±1	-42±3	-10±1	+34±1
Expansion velocity v_{exp} (km s ⁻¹)	11	15	10	11
Kinematical distance (kpc)	1.0	3.0±1.0	3.3±1.0	3.0±0.5
Adopted distance (kpc)	0.5±0.1	3.5±1.0	3.5±1.0	3.0±0.6
Radius of the HI cavity R_{cav}	1°6	1°25	0°6	0°6
Radius of the HI structure R_s	3°0	1°9	1°2	1°5
Radius of the HI structure R_s (pc)	26±5	116±33	70±20	52±9
Mass in the shell (M_{\odot})	600±240	58800±33600	4300±2450	6900±2300
Mass deficiency (M_{\odot})	80±32	6000±3400	1100±630	350±120
Swept-up mass M_s (M_{\odot})	340±140	32400±18500	2700±1540	3600±1200
n_e (cm ⁻³) (f=1.0)	...	0.5	...	0.9
M_i (M_{\odot}) (f=1.0)	...	24000	...	2900
n'_e (cm ⁻³) (f=0.3)	...	0.9	...	1.8
M'_i (M_{\odot}) (f=0.3)	...	13200	...	1600
Kinetic energy (10 ⁴⁸ erg)	0.4	73–103	2.7	4.4–6.3
Dynamical age (10 ⁶ yr)	1.2	4.3	3.5	3.8
Ambient density n_o (cm ⁻³)	0.2	0.2–0.3	0.08	0.25–0.35

(e.g. Green 2004) distances derived from the Σ -D relation are hardly reliable. Both SNRs are detected at 35 MHz (Dwarakanath & Udaya-Shankar 1990). An inspection of the image at 4850 MHz shows weak emission, also probably related to these remnants. Two different facts can be proposed as the origin of the HI cavity. On one hand, the HI cavity and shell can be associated with the SNRs, as was found in many SNRs (e.g. Paron et al. 2006; Reynolds et al. 2008). In this case its systemic velocity of +36 km s⁻¹ suggests near and far kinematical distances of 3.2 and 13 kpc, respectively. On the other hand, if the HI hole originates in absorption due to the radio continuum sources, then the distance to the SNRs can be inferred from the highest positive velocity at which the hole is detected (about +52 km s⁻¹). This suggests that the SNRs are placed at distances ≥ 4.5 kpc. Further data are necessary to elucidate this question.

CO emission (Dame et al. 2001) is present mainly at $b > -3^\circ$. The integrated CO emission (not shown here) in a velocity range similar to that of the HI emission does not show molecular material linked to the hole at $(l, b) = (17^\circ 5, -2^\circ 7)$. Weak CO emission present in the interval +28.0 to +43.6 km s⁻¹ encircles the border of the cavity related to the SNRs towards $b > -3^\circ$.

6. DISCUSSION

6.1. Physical parameters

The main physical parameters of the neutral gas structures linked to the O-type stars are summarized in Table 2. The (l, b) centers correspond to the approximate centroid of the features. The velocity interval indicates the velocity range where the HI structures can be identified, v_1 and v_2 being the lowest and highest velocities, respectively, at which the features are detected.

Following Cappa et al. (2008), the expansion velocities were estimated as $v_{\text{exp}} = (v_2 - v_1)/2 + 1.3$ km s⁻¹. The derived values are lower limits since the caps of the expanding shells are not detected in the present cases. The extra 1.3 km s⁻¹ takes into account the fact that the caps may be present just outside the velocity range at which the HI cavity is detected, that is at velocities $v_1 - 1.3$ km s⁻¹ and $v_2 + 1.3$ km s⁻¹.

For the four selected stars the adopted distances are compatible with the spectrophotometric and kinematical distance estimates. Uncertainties in the adopted kinematical distances for HD 124979, HD 163758, and HD 171589 arise in a velocity dispersion of ± 6 km s⁻¹ adopted for our Galaxy.

The radius of each cavity corresponds to the geometric mean of the major and minor semiaxes, while

TABLE 3
ENERGETICS OF THE STRUCTURES

	HD 38666	HD 124979	HD 163758	HD 171589
$T_{\text{eff}}^{\text{a}}$	34600	37100	40200	40000
$\log L (L_{\odot})$	5.0	5.6	6.03	5.7
$M (M_{\odot})$	23	40	70	47
$\dot{M} (10^{-6} M_{\odot} \text{ yr}^{-1})$	0.00032 ^b –0.005 ^c 0.02 ^d –0.35 ^e	1.8 ^e	8.3 ^e	2.7 ^e
$V_{\infty} (\text{km s}^{-1})$	1200 ^b	2100 ^f	2400 ^f	2500 ^f
$L_w (10^{36} \text{ erg s}^{-1})$	0.0002–0.16	2.5	15.0	5.4
Dynamical age (10^6 yr)	1.2	4.3	3.5	3.8
$E_w (10^{48} \text{ erg})$	0.008–6.0	350	1660	660
ϵ	50–0.07	0.2–0.3	0.002	0.007–0.01
Stellar lifetime ^g (10^6 yr)	7.0	4.5	3.0	4.0

^aVacca et al. (1996).

^bMartins et al. (2005).

^cChlebowski & Garmany (1991).

^dHowarth & Prinja (1989).

^eEstimated from Vink, de Koter, & Lamers (2000).

^fAdopted from Prinja, Barlow, & Howarth (1990).

^gSchaller et al. (1992).

the radii of the HI shells (R_s) were evaluated from the position of the maxima in the envelopes. Errors in the radii arise from the distance uncertainty.

Neutral atomic masses in the shells and mass deficiencies in the cavities are also listed in Table 2. The structures surrounding HD 124979 and HD 171589 are easier to define over the halves further away from the galactic plane. In each case, the other half is contaminated with diffuse emission from the galactic plane. Thus, for these two structures, the neutral mass in the shells was derived as twice the mass associated with the better defined half. The swept-up neutral masses were obtained as mean values between the neutral mass deficiency in the voids and the neutral mass in the envelopes. This procedure allows us to remove a first order contribution of the background emission, since both mass determinations are probably contaminated with neutral gas unrelated to the structures. Values listed in Table 2 include a typical interstellar He abundance of 10%.

In the previous sections we have stated that no radio continuum emission associated with the HI structures was detected. Assuming that the massive stars have ionized the surrounding gas through their strong UV photon flux, and that this ionized material has been swept-up and is present in the inner borders of the neutral envelopes, we can derive an upper limit for the electron density n_e and the ion-

ized mass M_i from the rms flux density at 4.85 GHz (7.7 mJy beam⁻¹). Adopting $R_{\text{out}} = 1.0 R_{\text{cav}}$ and $R_{\text{in}} = 0.9 R_{\text{cav}}$ as the outer and inner radii of the ionized regions, we estimated upper limits for the flux densities $S_{4.85\text{GHz}} = 3.7$ and 1.0 Jy for the ionized regions around HD 124979 and HD 171589, respectively. Estimates of the physical parameters of the HII regions towards these stars can be obtained using the expressions by Mezger & Henderson (1967) for spherical ionized regions of constant density. Adopting an electron temperature of 8×10^3 K and a volume filling factor $f = 1.0$, we derived the electron density n_e and the associated ionized mass M_i . A different electron density and ionized mass can be estimated by considering an alternative filling factor. For an ionized shell with outer and inner radii of R_{out} and R_{in} , in which the plasma covers an area A equal to 50% of the surface of the shell, the filling factor can be derived as $f = A \times (R_{\text{out}}^3 - R_{\text{in}}^3) / R_{\text{out}}^3 = 0.3$. This value was used to derive n'_e and M'_i . The derived values for n'_e are consistent with the high z -distances of the stars. Note that electron densities and ionized masses are upper limits. Unfortunately, the lack of radio data at frequencies higher than 1 GHz precludes the derivation of upper limits for the regions of HD 38666 and HD 163758.

The kinetic energy $E_k = M_b v_{\text{exp}}^2 / 2$ was estimated from the expansion velocities listed in Ta-

ble 2 and the neutral and ionized masses in the structures. The range in kinetic energies corresponds to the fact that we have taken into account the neutral atomic mass only, and the neutral atomic and ionized masses.

Dynamical ages were estimated as $t_d = 0.55 \times 10^6 R_s / v_{\text{exp}}$ yr (McCray 1983), where R_s is the radius of the bubble (pc), v_{exp} is the expansion velocity (km s^{-1}), and the constant represents a mean value between the energy and the momentum conserving cases.

Finally, ambient densities n_o were derived by uniformly distributing the associated mass within a sphere of radius R_s . For the regions of HD 124979 and HD 171589 two values are listed in Table 2. The first one was obtained by distributing the swept-up neutral mass (M_s) while the second one was derived by distributing the neutral and ionized masses ($M_s + M_i$). The major source of error in radii and masses is the distance uncertainty. The low ambient densities are consistent with the structures being far from the galactic plane.

6.2. Energetics and origin of the structures

We will analyze here whether the massive stars can provide the energy to create the cavities and shells found in the previous sections through their stellar winds and UV photon fluxes. To test the former possibility, we will estimate the mechanical energy E_w released into the ISM for the massive stars and compare it with the kinetic energy E_k of the structures.

Table 3 summarizes relevant parameters useful to evaluate the energetics of the structures. The values of the effective temperature T_{eff} , the stellar luminosity L , and the stellar mass listed in the first three rows correspond to the spectral classification and luminosity class of the O-type stars listed in Table 1. These data were used to derive the mass loss rate \dot{M} following the recipe by Vink et al. (2000). Based on the mass loss rates and terminal velocities, we estimated the mechanical wind luminosity for each star as $L_w = \dot{M} V_w^2 / 2$.

The stellar wind mechanical energy $E_w (= L_w t)$ released by the massive stars was derived from the dynamical ages of the bubbles. The resulting values are included in Table 3.

The ratio ϵ between the kinetic energy E_k and the mechanical energy E_w provided by the massive stars during the dynamical age of the structures is also included in Table 3. Evolutionary models of stellar wind bubbles predict that $\epsilon = 0.2$ for the energy conserving case and $\epsilon \leq 0.1$ for the momentum con-

serving case (see McCray 1983). Although the uncertainty in this value is large (at least 70% adopting a 30% error in the distance), it is clear that HD 163758 and HD 171589 are capable of blowing the observed structures. The result for HD 124979 is still consistent with an interstellar bubble interpretation.

The obtained dynamical ages for HD 124979, HD 163758, and HD 171589 are compatible with the ages derived from evolutionary tracks for stars with solar abundances (see Schaller et al. 1992).

The case for HD 38666 is more complex. The large uncertainty in the estimated mechanical energy does not allow a clear conclusion about the origin of this structure. The derived dynamical age is lower than the age estimate obtained from Schaller et al. (1992). However, Martins et al. (2005) estimate an age $< (2-4) \times 10^6$ yr, closer to the dynamical age. On the other hand, Hoogerwerf, de Bruijne, & de Zeeuw (2001) proposed a binary-binary collision between three stars of Trapezium cluster: AE Aur, HD 38666, and ι Ori, becoming HD 38666 and AE Aur runaway stars. The dynamical ejection scenario took place 2.5×10^6 yr ago. We note that a search for other catalogued massive stars at a distance compatible with that of the structure gave negative results. A different analysis can be done bearing in mind the observed proper motions. HD 38666 and HD 124979 have large spatial velocities, about $57 \pm 11 \text{ km s}^{-1}$ for HD 38666, and $200 \pm 30 \text{ km s}^{-1}$ for HD 124979. Considering these velocities, which include the uncertainty in the adopted distance, it took HD 38666 about $(0.4-0.9) \times 10^6$ yr to cross the HI structure. As regards HD 124979, the time necessary to cross the structure was about $(0.6-1.0) \times 10^6$ yr. Adopting 0.7×10^6 yr for HD 38666 and 0.8×10^6 yr for HD 124979, the mechanical energy turns out to be $(0.004-3.5) \times 10^{48}$ erg for HD 38666 and 65×10^{48} erg for HD 124979. The large spatial velocity of the runaway star HD 124979 shortens the crossing time through the structure, so their origin remains unclear. The resulting ϵ -values indicate that other energy sources are necessary to create both structures through the stellar wind mechanism. Additional studies are necessary to identify the agents.

No bow-shock like features were found related to HD 38666 and HD 124979. As shown by Raga et al. (1997) and Huthoff & Kaper (2001), bow-shocks appear associated with only about 30–40% of the OB runaway stars. As indicated by the last authors, large separations from the galactic plane, extremely high space velocities and large distances make difficult the formation and detection of bow-shock structures. Moreover, the physical conditions

of the ambient medium where the star is immersed play a major role in determining the existence of bow-shocks. Particularly, these authors find an anticorrelation between bow-shocks and hot bubbles. Whether or not the observed structures originate in the mass flow of the massive stars, the lack of bow-shocks in these cases is consistent with their conclusions.

Taking into account the spectral classification and the luminosity class of the associated massive stars and the ambient density where the structures are evolving, the estimated radius of the Strömgen's spheres is in all cases larger than the HI cavities. The smaller size of the cavities can be explained taking into account that a certain number of UV photons are used in dust heating, or drain from the patchy envelopes.

7. SUMMARY

We have analyzed the interstellar medium in the environs of the O-type stars HD 38666, HD 124979, HD 163758, and HD 171589. The study of the neutral hydrogen distribution in direction to these stars allowed us to reveal HI structures located at kinematical distances compatible with the stellar distances and probably related to the stars.

Assuming a stellar wind mechanism, the derived dynamical ages for the HI structures related to HD 124979, HD 163758, and HD 171589 are compatible with the lifetimes of the O-type stars on the main sequence, reinforcing the association with the stars.

We have investigated the counterparts of the structures at other frequencies. The surrounding HI shells around HD 38666, HD 124979, and HD 171589 have IR counterparts, revealing the presence of dust associated with the HI gas. The HI shell related to HD 163758 has IR and H α counterparts, with the star projected onto one of its higher density borders.

To investigate the origin of the structures, we have compared the mechanical energy released into the ISM by the massive stars and the kinetic energy of the structures. Our results for the energy conversion efficiency for HD 163758 and HD 171589 indicate that the stars are capable of blowing the observed structures. As regards HD 38666 and HD 124979, additional energy sources are probably necessary, taking into account the derived ϵ -values and the large tangential velocities. Additional studies are needed to clarify their origin.

We thank Dr. P. Benaglia for her help in the first stages of this paper. We also thank Dr. J. C. Testori for his collaboration. It is a pleasure to thank the

anonymous referee for many comments and suggestions that improved this presentation. This project was partially financed by the Consejo Nacional de Investigaciones Científicas y Técnicas (CONICET) of Argentina under project PIP 5886/05, Agencia PICT 14018, and UNLP under projects 11/G072. We acknowledge the use of NASA's SkyView facility (<http://skyview.gsfc.nasa.gov>) located at NASA Goddard Space Flight Center. The reduction and analysis of the PMN Survey data was largely the work of Mark Griffith and Alan Wright. The FITS maps of the PMN Survey were produced by Jim Condon (NRAO) and Niven Tasker. This research has made use of the SIMBAD database, operated at CDS, Strasbourg, France.

REFERENCES

- Arnal, E. M., Bajaja, E., Larrarte, J. J., Morras, R., & Pöppel, W. G. L. 2000 *A&AS*, 142, 35
- Arnal, E. M., Cappa, C. E., Rizzo, J. R., & Cichowolski, S. 1999, *AJ*, 118, 1798
- Blaauw, A. 1961, *Bull. Astron. Inst. Netherlands*, 15, 265
- Brand, J., & Blitz, L. 1993, *A&A*, 275, 67
- Cappa, C. E., & Benaglia, P. 1998, *AJ*, 116, 1906
- Cappa, C. E., Niemela, V. S., Amorín, R., & Vásquez, J. 2008, *A&A*, 477, 173
- Cappa, C. E., Rubio, M., Martín, M. C., & McClure-Griffiths, N. M. 2005, in *ASP Conf. Ser. 344, The Cool Universe: Observing Cosmic Dawn*, ed. D. Lidman & C. Alloin (San Francisco: ASP), 179
- Chlebowski, T., & Garmany, C. D. 1991, *ApJ*, 368, 241
- Cichowolski, S., & Arnal, E. M. 2004, *A&A*, 414, 203
- Condon, J. J., Griffith, M. R., & Wright, A. E. 1993, *AJ*, 106, 1095
- Dame, T. M., Hartmann, D., & Thaddeus, P. 2001, *ApJ*, 574, 792
- Dwarakanath, K. S., & Udaya-Shankar, N. 1990, *J. Astrophys. Astron.*, 11, 323
- Finkbeiner, D. P. 2003, *ApJS*, 146, 407
- Garmany, C. D., Conti, P. S., & Chiosi, C. 1982, *ApJ*, 263, 777
- Goss, W. M., & Lozinskaya, T. A. 1995, *ApJ*, 439, 637
- Green, D. A. 2002, *VizieR Online Data Catalog 7227*, 0
- _____. 2004, *Bull. Astron. Soc. India*, 32, 335
- Guseinov, O. H., Ankay, A., & Tagieva, S. O. 2003, *Serb. Astron. J.*, 167, 93
- Haslam, C. G. T., Salter, C. J., Stoffel, H., & Wilson, W. E. 1982, *A&AS*, 47, 1
- Høg, E., et al. 2000, *A&A*, 355, 27
- Hoogerwerf, R., de Bruijne, J. H. J., & de Zeeuw, P. T. 2001, *A&A*, 365, 49
- Howarth, I. D., & Prinja, R. K. 1989, *ApJS*, 69, 527
- Huthoff, F., & Kaper, L. 2001, in *Black Holes in Binaries and Galactic Nuclei*, ed. L. Kaper, E. P. J. van den Heuvel & P. A. Woudt (Berlin: Springer-Verlag), 314

- Kalberla, P. M. W., Burton, W. B., Hartmann, D., Arnal, E. M., Bajaja, E., Morras, R., & Pöppel, W. G. L. 2005, *A&A*, 440, 775
- Kozok, J. R. 1985, *A&AS*, 62, 7
- Lozinskaya, T. A. 1982, *Ap&SS*, 87, 313
- MacConnell, D. J., & Bidelman, W. P. 1976, *AJ*, 81, 225
- Maíz-Apellániz, J., Walborn, N. R., Galue, H. A., & Wei, L. H. 2004, *VizieR Online Data Catalog*, 5116, 0
- Martins, F., Schaerer, D., Hillier, D. J., Meynadier, F., Heydari-Malayeri, M., & Walborn, N. R. 2005, *A&A*, 441, 735
- Mason, B. D., Gies, D. R., Hartkopf, W. I., Bagnuolo, Jr., W. G., ten Brummelaar, T., & McAlister, H. A. 1998, *AJ*, 115, 821
- McCray, R. 1983, *Highlights Astron.*, 6, 565
- Mezger, P. G., & Henderson, A. P., 1967, *ApJ*, 147, 471
- Miville-Deschênes, M. A., & Lagache, G. 2005, *ApJS*, 157, 302
- Nazé, Y., Chu, Y.-H., Guerrero, M. A., Oey, M. S., Gruendl, R. A., & Smith, R. C. 2002, *AJ*, 124, 3325
- Olano, C. A. 1982, *A&A*, 112, 195
- Paron, S. A., Reynoso, E. M., Dubner, G. M., & Purcell, C. 2006, *RevMexAA (SC)*, 26, 164
- Prinja, R. K., Barlow, M. J., & Howarth, I. D. 1990, *ApJ*, 361, 607
- Raga, A. C., Noriega-Crespo, A., Cantó, J., Steffen, W., van Buren, D., Mellema, G., & Lundqvist, P. 1997, *RevMexAA*, 33, 73
- Reynolds, S. P., Borkowski, K. J., Green, D. A., Hwang, U., Harrus, I., & Petre, R. 2008, *ApJ*, 680, L41
- Russeil, D. 2003, *A&A*, 397, 133
- Schaller, G., Schaerer, D., Meynet, G., & Maeder, A. 1992, *A&AS*, 96, 269
- Vacca, W. D., Garmany, C. D., & Shull, J. M. 1996, *ApJ*, 460, 914
- van Buren, D., & McCray, R. 1988, *ApJ*, 329, L93
- van der Hucht, K. A. 2001, *NewA Rev.*, 45, 135
- Vink, J. S., de Koter, A., & Lamers, H. J. G. L. M. 2000, *A&A*, 362, 295
- Walborn, N. R. 1971, *ApJS*, 23, 257
- Weaver, R., McCray, R., Castor, J., Shapiro, P., & Moore, R. 1977, *ApJ*, 218, 377
- Wegner, W. 1994, *MNRAS*, 270, 229
- Wilkin, F. P. 1996, *ApJ*, 459, L31

C. E. Cappa and G. A. Romero: Instituto Argentino de Radioastronomía, Parque Pereyra Iraola Km 40, 500, CC 5, Villa Elisa, Buenos Aires, Argentina and Facultad de Ciencias Astronómicas y Geofísicas, Universidad Nacional de la Plata, Paseo del Bosque s/n, 1900, La Plata, Buenos Aires, Argentina (cappa@fcaglp.unlp.edu.ar).

M. C. Martín: Instituto Argentino de Radioastronomía, Parque Pereyra Iraola Km 40, 500, CC 5, Villa Elisa, Buenos Aires, Argentina (cmartin@iar.unlp.edu.ar).